Sensorless Position and Speed Control of IPMSM with Sliding Mode Observer and Voltage Signal Injection

Ertugrul Ates
Dept. of Electrical and Electronics Eng.
Abdullah Gul University
Kayseri, Turkey
ertugrul.ates@agu.edu.tr

Burak Tekgun
Dept. of Electrical and Electronics Eng.
Abdullah Gul University
Kayseri, Turkey
burak.tekgun@agu.edu.tr

Gunyaz Ablay
Dept. of Electrical and Electronics Eng.
Abdullah Gul University
Kayseri, Turkey
gunyaz.ablay@agu.edu.tr

2021 3rd Global Power, Energy and Communication Conference (GPECOM) | 978-1-6654-3512-3/21/$31.00 ©2021 IEEE | DOI: 10.1109/GPECOM52585.2021.9587579

***Abstract*—A sensorless control approach based on a sliding mode observer for predicting the rotor position and speed is studied in this work. For predicting the motor speed and position, the sliding mode observer followed by a phase locked loop is formulated by means of the back EMF model. The voltage signal injection method is utilized for accurate estimation in zero or low speed region. Numerical simulation results are provided for an 8-pole IPMSM, which shows that the motor speed and position in zero or low-speed region are accurately estimated with the designed observer and voltage signal injection approach.**

Keywords—synchronous machine, voltage signal injection, sliding-mode observer, phase-locked loop, sensorless control

I. INTRODUCTION

The interior permanent magnet synchronous machines (IPMSMs) are commonly utilized in industrial applications because of their attractive features like having a good dynamic performance, operating with high efficiency at a wide speed range and operating at a high power factor with a high power density. IPMSMs are mostly controlled with field-oriented control (FOC) approach which is basically relying on the phase current, motor speed, and position feedbacks to be acquired accurately. However, if the mechanical sensor is used, it will cause increasing cost, size, and reliability problems. To overcome these problems, sensorless control methods are preferred. Several estimation methods to get the motor speed and position information without the usage of physical sensors have been studied in recent years. The sensorless speed estimation methods that use back electromotive force (EMF) estimation are categorized as the flux observer, the disturbance observer, the Kalman filter, the sliding mode observer (SMO), and model reference adaptive control (MRAC) methods [1]–[3]. Compared to the other estimation methods, SMO is commonly utilized due to its various attractive features including reliability, desired performance, and robustness against system parameter variations. In practical applications, to eliminate the possible chattering problem, which is inherent in SMOs, the discontinuous signum function is smoothed with a sigmoidal, saturation or tangent hyperbolic function in the SMO designs [4]–[6].

During the motor operations at zero or low speed, it is not easy to estimate the motor speed/position accurately by means of back EMF as it gets very small amplitude values to be detected. Nonetheless, the signal injection approach can be applied to the stator voltage or current references for getting the error-free motor speed/position in the zero or low-speed region [7]–[9]. There are two types of signal injection approaches that are named as the rotating [10] and the pulsating signal injection approaches [11] by considering the types of the carrier signals. Other than these, the bidirectional rotating carrier signal injection approach is also studied in [12] to optimize system delays, inverter nonlinearities, and stator resistance. In this method, two carrier voltages with distinct frequencies are injected simultaneously. To get the speed/position information from the predicted system states such as back EMF after signal injection, several different methods have been used [13], [14].

The classical arc-tangent function is commonly used to calculate the position information from the back EMF states in many studies. However, the precision of the position estimation can be disturbed due to the presence of harmonics and noise. In particular, there might be an estimation error by computing the arc-tangent function owing to the noise if the back EMF intersects zero. To eliminate this issue, the phase-locked loop (PLL) method is generally utilized in industrial applications [15]. In this method, the estimated back EMF signal is adopted to the motor position. Furthermore, several researches based on the SMO and PLL are reported in the literature in order to acquire motor speed and position estimations. In [16], [17], the quadrature PLL method is introduced to eliminate the negative sign of speed in the back EMF. The conventional PLL method is utilized in [18], [19]. In addition, to eliminate the effects of the phase lag and high-frequency signal in the back EMF, a PLL scheme with tangent function is studied in [20].

In this study, a voltage signal injection-based SMO and PLL structure are proposed to achieve sensorless control in the IPMSMs. Firstly, the SMO structure is designed to get the estimated currents in the α-β reference domain. To eliminate a possible chattering issue, a smooth sigmoid function is utilized in SMO implementation in place of the discontinuous signum function. Then, the motor speed and position are acquired by using a PLL. Hence, not only the estimations got more accurate but also division to zero problems are eliminated comparing with the arctangent calculation. Comparing with the other sensorless control techniques, the proposed method improves the sensorless control performance by having highly accurate speed and position estimations in high, low, and zero speed, and improves the system stability for a wide range of speed and loading conditions.

The paper organization is as follows. The general information of the FOC structure of the IPMSM and mathematical model is given in Section II. The SMO method and the PLL structure are presented in Section III. The voltage

978-1-6654-3512-3/21/$31.00 ©2021 IEEE

signal injection method is given in Section IV. Numerical simulation results are presented in Section V and the final conclusions of the study are given in Section VI.

II. The IPMSM Control Scheme

A. FOC Structure of the IPMSM

The FOC structure for the IPMSM is illustrated in Fig. 1. In this system, the SMO is used for achieving the sensorless control system, and the SMO model is designed by utilizing the back EMF model together with a PLL model for estimating the rotor position/speed.

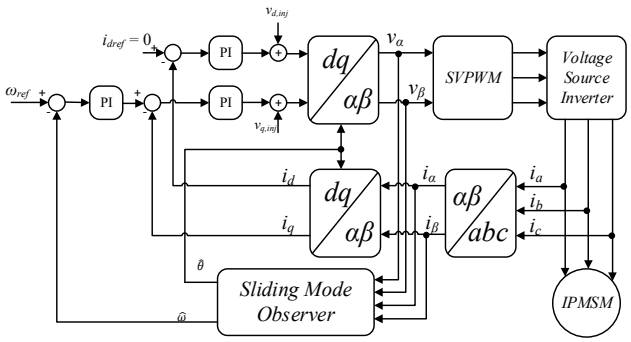

Fig. 1. The sensorless FOC structure of the IPMSM system.

IPMSM consists of a three-phase stator winding (a, b, c axes), and permanent magnets (PM) rotor for excitation. The motor is controlled by a standard six switch three-phase inverter. In order to produce the phase currents in the FOC structure, the space vector pulse width modulation (SVPWM) technique is used to generate the gating signals as shown in Fig. 2.

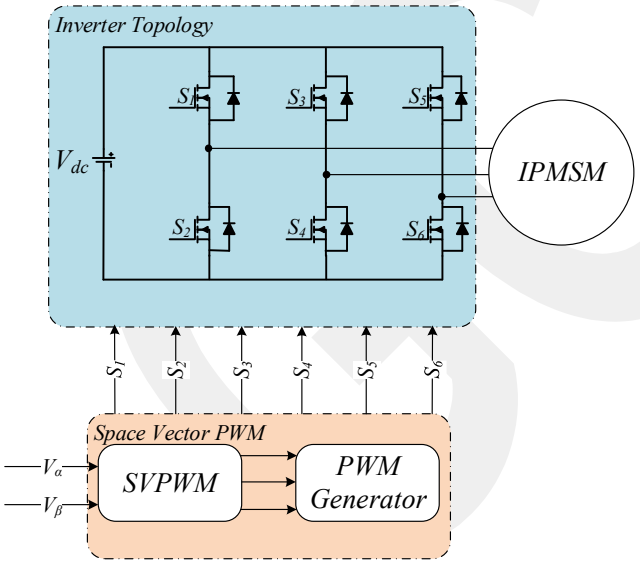

Fig. 2. The SVPWM scheme and the inverter topology

B. The IPMSM System Model

The designed back EMF model of the sensorless IPMSM control system based on SMO is given by

$$\begin{bmatrix} u_\alpha \\ u_\beta \end{bmatrix} = \begin{bmatrix} R_s + DL_d & \omega_e(L_d - L_q) \\ -\omega_e(L_d - L_q) & R_s + DL_q \end{bmatrix} \begin{bmatrix} i_\alpha \\ i_\beta \end{bmatrix} + \begin{bmatrix} e_\alpha \\ e_\beta \end{bmatrix} \quad (1)$$

$$\begin{bmatrix} e_\alpha \\ e_\beta \end{bmatrix} = \left[(L_d - L_q)(\omega_e i_d - \dot{i_q}) + \omega_e \psi_f \right] \begin{bmatrix} -\sin\theta_e \\ \cos\theta_e \end{bmatrix} \quad (2)$$

where u_α, u_β are the applied voltages and i_α, i_β are currents in the stationary d-q reference frame (α-β), R_s is the phase winding resistance, L_d and L_q are the synchronous inductances, θ_e and ω_e are the motor electrical position and speed, D represents the differential operator, e_α and e_β represent the back EMF components in the stationary d-q reference frame, and ψ_f is the of the PM flux linkage.

IPMSM state equation can be written by considering the back EMF equation in the following form.

$$\begin{bmatrix} \dot{i_\alpha} \\ \dot{i_\beta} \end{bmatrix} = \begin{bmatrix} -R_s/L_d & -\omega_e(L_d - L_q)/L_d \\ \omega_e(L_d - L_q)/L_d & -R_s/L_d \end{bmatrix} \begin{bmatrix} i_\alpha \\ i_\beta \end{bmatrix} + \frac{1}{L_d} \begin{bmatrix} u_\alpha \\ u_\beta \end{bmatrix} - \begin{bmatrix} 1/L_d & 0 \\ 0 & 1/L_d \end{bmatrix} \begin{bmatrix} e_\alpha \\ e_\beta \end{bmatrix} \quad (3)$$

Model (3) is represented in terms of stator currents for use in the observer design.

III. PLL Structure with SMO

A. Design of the SMO

The SMO shown in Fig. 3 is designed for predicting the motor velocity and position. The SMO structure for the IPMSM system (3) in the $\alpha - \beta$ reference domain can be written as

$$\begin{bmatrix} \dot{\hat{i}_\alpha} \\ \dot{\hat{i}_\beta} \end{bmatrix} = \begin{bmatrix} -R_s/L_d & -\hat{\omega}_e(L_d - L_q)/L_d \\ \hat{\omega}_e(L_d - L_q)/L_d & -R_s/L_d \end{bmatrix} \begin{bmatrix} \hat{i}_\alpha \\ \hat{i}_\beta \end{bmatrix} + \frac{1}{L_d} \begin{bmatrix} u_\alpha \\ u_\beta \end{bmatrix} - \begin{bmatrix} 1/L_d & 0 \\ 0 & 1/L_d \end{bmatrix} \begin{bmatrix} k_1 F(\hat{i}_\alpha - i_\alpha) \\ k_2 F(\hat{i}_\beta - i_\beta) \end{bmatrix} \quad (4)$$

where $\hat{i}_\alpha$ and $\hat{i}_\beta$ are the estimated currents, k_1 and k_2 are the observer gains and $F(x)$ represents the sigmoid function. Conventionally, in the SMO structure, the sign function is used, but its discontinuous nature causes chattering issues. To overcome the chattering issue, the continuous sigmoid function is preferred, which is given by

$$F(x) = \frac{(1 - e^{-\alpha x})}{(1 + e^{-\alpha x})} \quad (5)$$

where α is an adjustable constant, by subtracting (3) from (4) and defining as $\tilde{i_\alpha} = \hat{i}_\alpha - i_\alpha$ and $\tilde{i_\beta} = \hat{i}_\beta - i_\beta$ as state errors, the error equation is obtained as

$$\begin{aligned} \dot{\tilde{i_\alpha}} &= (-R_s/L_d)\tilde{i_\alpha} - \left(\frac{L_d - L_q}{L_d}\right)(\hat{\omega}_e \hat{i_\beta} - \omega_e i_\beta) + \frac{e_\alpha}{L_d} - \frac{k_1 F(\tilde{i_\alpha})}{L_d} \\ \dot{\tilde{i_\beta}} &= (-R_s/L_d)\tilde{i_\beta} + \left(\frac{L_d - L_q}{L_d}\right)(\hat{\omega}_e \hat{i_\alpha} - \omega_e i_\alpha) + \frac{e_\beta}{L_d} - \frac{k_2 F(\tilde{i_\beta})}{L_d} \end{aligned} \quad (6)$$

By defining the sliding surfaces from the state error as

$$S(X) = \begin{bmatrix} \hat{i}_\alpha - i_\alpha \\ \hat{i}_\beta - i_\beta \end{bmatrix} = \begin{bmatrix} \tilde{i}_\alpha \\ \tilde{i}_\beta \end{bmatrix} \tag{7}$$

A Lyapunov function for analyzing the stability can be defined as

$$V = S(X)^T S(X) = \frac{\tilde{i}_\alpha^{\,2} + \tilde{i}_\beta^{\,2}}{2} \tag{8}$$

From time derivative of (8), the SMO stability is obtained as

$$\dot{V} = \tilde{i}_\alpha \dot{\tilde{i}}_\alpha + \tilde{i}_\beta \dot{\tilde{i}}_\beta \le 0 \tag{9}$$

By simplifying (9), the equation can be obtained as

$$\dot{V} = \frac{-R_s}{L_d}\left(\tilde{i}_\alpha^{\,2} + \tilde{i}_\beta^{\,2}\right) + \frac{e_\alpha \tilde{i}_\alpha + e_\beta \tilde{i}_\beta}{L_d} - \frac{k_1 F(\tilde{i}_\alpha)\tilde{i}_\alpha}{L_d} - \frac{k_2 F(\tilde{i}_\beta)\tilde{i}_\beta}{L_d} \tag{10}$$

In order for the stable operation of the SMO, the observer gain k_1 and k_2 should be large enough to hold $k_1 > \max(|e_\alpha|)$ and $k_2 > \max(|e_\beta|)$. Then $\dot{V} \le 0$ which indicates error convergence to zero. This means that, once the state errors reach zero, the sliding surfaces are also satisfy$\dot{S}(X) = S(X) = 0$. Then, the back-EMF can be estimated as

$$\begin{aligned} \hat{e}_\alpha &= k_1 F(\hat{i}_\alpha - i_\alpha) \\ \hat{e}_\beta &= k_2 F(\hat{i}_\beta - i_\beta) \end{aligned} \tag{11}$$

These back-EMF estimations can be used with a PLL model to estimate the motor angular velocity and position.

B. Rotor Position Estimation with PLL

The PLL structure used with SMO is illustrated in Fig. 3. In conventional SMO designs, the arctangent of the estimated back-EMF values is used to calculate the position of the rotor. Nevertheless, the accuracy of the position and velocity estimations are affected due to the existence of noise and harmonic components. To eliminate this issue, the PLL model can be used for velocity and position estimations in the sensorless control structure of the IPMSM.

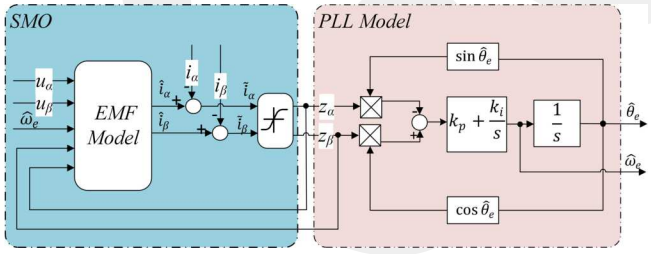

Fig. 3. SMO and PLL structure.

The conventional PLL integrated into the SMO is shown in Fig. 3. Since $z_\alpha = E\cos\theta_e$, $z_\beta = E\sin\theta_e$ and $E \approx \omega_e \lambda_f$, the following PLL error equation is obtained:

$$\begin{aligned} E\sin\theta_e\cos\hat{\theta}_e - E\cos\theta_e\sin\hat{\theta}_e &= E\sin(\theta_e - \hat{\theta}_e) \\ &\approx E(\theta_e - \hat{\theta}_e) \end{aligned} \tag{12}$$

where the small angle approximation is used. Hence, the PLL transfer function in s-domain can be obtained as

$$\frac{\hat{\theta}_e}{\theta_e} = \frac{Ek_p s + Ek_i}{s^2 + Ek_p s + Ek_i} \tag{13}$$

where k_p and k_i are the proportional and the integral gains of the standard PI regulator.

As seen on the Bode diagram of the traditional PLL displayed in Fig. 4, if the rotating speed changes, then only the bandwidth of the PLL varies with appropriate PI regulator parameters.

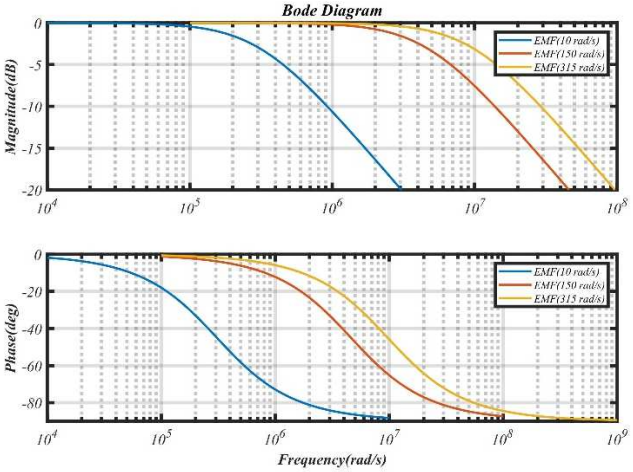

Fig. 4. The Bode plots of the PLL structure for different speeds.

IV. Voltage Signal Injection Approach

A vectorized voltage signal added into the estimated synchronous reference frame (SynRF) is given as

$$\begin{bmatrix} \hat{v}_{d,inj} \\ \hat{v}_{q,inj} \end{bmatrix} = \begin{bmatrix} V_{inj}\cos\omega_{inj}t \\ 0 \end{bmatrix} \tag{14}$$

where the $\hat{v}_{d,inj}$ and $\hat{v}_{q,inj}$ are the voltage signals injected into estimated SynRF, V_{inj} represents the signal amplitude and ω_{inj} is the signal frequency.

When the motor is operated close to or at zero speed region and the voltage is added with a high enough frequency and amplitude, then it is possible to ignore the resistive voltage drop and back EMF. So, the terminal equation of the IPMSM in the stationary reference frame is

$$\begin{bmatrix} v_\alpha \\ v_\beta \end{bmatrix} = \begin{bmatrix} L_{avr} + L_{dif}\cos 2\theta_r & L_{dif}\sin 2\theta_r \\ L_{dif}\sin 2\theta_r & L_{avr} - L_{dif}\cos 2\theta_r \end{bmatrix} \frac{d}{dt}\begin{bmatrix} i_\alpha \\ i_\beta \end{bmatrix} \tag{15}$$

where u_α, u_β are the voltages and i_α, i_β are currents in the stationary d-q reference frame, θ_r represents the motor position, $L_{avr} = (L_d + L_q)/2$ and $L_{dif} = (L_d - L_q)/2$.

Considering the injected voltage vector and voltage equation in the α-β frame, the response of the current excitation is given as

$$\begin{bmatrix}\hat{i}_{d,inj}\\ \hat{i}_{q,inj}\end{bmatrix} = \begin{bmatrix}L_{avr} - L_{dif}\cos 2\Delta\theta_r\\ -L_{dif}\sin 2\Delta\theta_r\end{bmatrix} \times \frac{V_{inj}\sin\omega_{inj}t}{\omega_{inj}(L_{avr}^2 - L_{dif}^2)} \quad (16)$$

where $\hat{i}_{d,inj}$, $\hat{i}_{q,inj}$ are the currents in estimated SynRF, $\Delta\theta_r = \theta_r - \hat{\theta}_r$ represents the position estimation error with the estimated position $\hat{\theta}_r$. Equation (16) clearly shows that the current fluctuates simultaneously with the added voltage signal phase, and indeed the voltage signal addition is used as an amplitude-based method.

V. Simulation Results

In order to verify the efficacy of the designed SMO and voltage signal injection-based sensorless control approach, a simulation study is conducted using MATLAB®/Simulink®. The IPMSM and control parameters are provided in Table I.

TABLE I. IPMSM Simulation Parameters

Parameters	Simulation Values
Stator Resistance R_s	1.2 Ω
d-axis Inductance L_d	8.5 mH
q-axis Inductance L_q	12.5 mH
Magnet Flux Linkage ψ_f	0.123 Wb
Pole number P	8
Observer gains k_1,k_2	400
PLL proportional gain k_p	250000
PLL integral gain k_i	0.0016
Sigmoid coefficient a	0.01
Bus Voltage V_{dc}	450 V

In this control mechanism, the SVPWM technique is implemented in the three-phase inverter. The actual motor velocity and position are obtained from the motor encoder, while they are also calculated from the proposed sensorless control system and compared. The load torque is applied by adjusting the reference quadrature axis current and the reference angular speed is varied from 0 to 315 rad/s. The injected voltage frequency, ω_{inj}, and the amplitude, $V_{inj,}$ are set to $2\pi180$ rad/s and 20 V, respectively.

The estimated and measured speed profiles are given in Fig. 5 (a). The load torque profile applied at the maximum speed region is displayed in Fig. 5 (b). The error in the speed estimation is presented in Fig. 5(c). It can be observed from the figures that the error between the actual and the estimated velocity is approximately zero. Moreover, the error between the actual and the estimated positions is below 1 % for most of the operation. The error reaches up to %7 in regions where the speed becomes zero. In such cases, it takes 0.4 seconds for the proposed observer to eliminate the estimation error.

The position estimations at 315 rad/s speed for the positive and negative directions are given in Fig. 6. One may observe that an accurate position estimation is obtained at the high-speed region.

The estimation results for the zero-speed region are shown in Fig. 7. (a) and the estimation error is shown in Fig. 7 (b). When the speed drops to zero, the estimation error settles to zero in about 0.4 seconds.

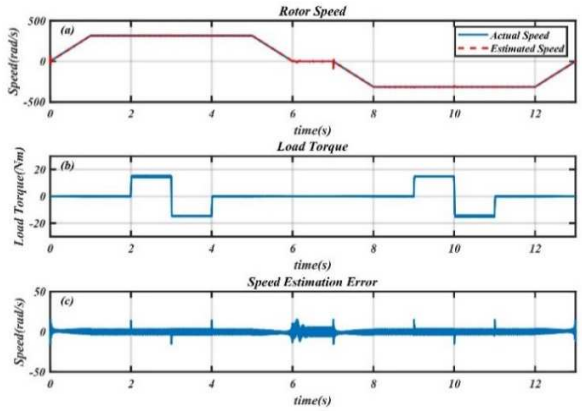

Fig. 5. (a) Actual and estimated speed profile, (b) load torque profile, (c) speed estimation error.

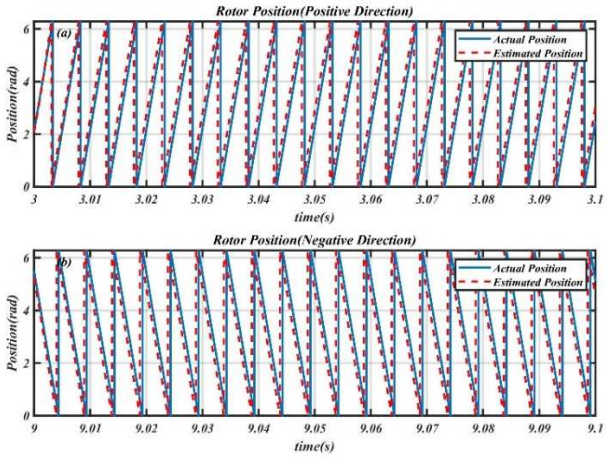

Fig. 6. The position estimation on (a) positive direction, (b) negative direction.

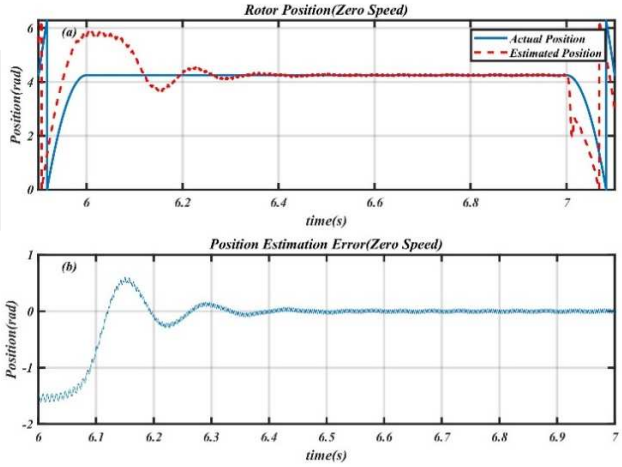

Fig. 7. (a) Position estimation and, (b) position estimation error in the zero-speed region.

VI. Conclusion

In this study, a sliding mode observer (SMO) with voltage signal injection approach is designed for estimating the motor speed and position of the IPMSM system. A phase-locked loop (PLL) mechanism is integrated into the SMO to improve the estimation accuracy of the velocity and the position and avoid the divide to zero problems of the arctangent calculation. To avoid the chattering problem, a continuous sigmoidal function is utilized in the observer implementation.

The SMO has the ability to handle nonlinear dynamics of the IPMSM for accurate state estimation in a wide range of operating regions. In addition, the voltage signal injection approach in the synchronous *d-q* frame is utilized for accurate estimation in zero or close to zero speed regions. The estimation approach is applied to an 8-pole IPMSM and numerical results are provided. Numerical results indicate that the designed estimation approach is able to fairly predict the rotor velocity and the position in high and low-speed regions with good dynamic performances. In future work, it is aimed to improve the estimation performance for the position estimation in the zero and close to zero speed regions by optimizing the signal injection approach and validating the efficacy of the proposed estimation method through experimental work.

REFERENCES

[1] S. M. Gadoue, D. Giaouris, J. W. Finch, and S. Member, "MRAS Sensorless Vector Control of an Induction Motor Using New Sliding Mode and Fuzzy Logic Adaptation Mechanisms," vol. 25, no. 2, pp. 394 - 402, 2009, doi: 10.1109/TEC.2009.2036445.

[2] F. Genduso, R. Miceli, C. Rando, and G. R. Galluzzo, "Back EMF sensorless-control algorithm for high-dynamic performance PMSM," *IEEE Transactions on Industrial Electronics*, vol. 57, no. 6, pp. 2092–2100, 2010, doi: 10.1109/TIE.2009.2034182.

[3] Z. Chen, M. Tomita, S. Doki, and S. Okuma, "An extended electromotive force model for sensorless control of interior permanent-magnet synchronous motors," *IEEE Transactions on Industrial Electronics*, vol. 50, no. 2, pp. 288–295, 2003, doi: 10.1109/TIE.2003.809391.

[4] G. Wang, Z. Li, G. Zhang, Y. Yu, and D. Xu, "Quadrature PLL-based high-order sliding-mode observer for IPMSM sensorless control with online MTPA control strategy," *IEEE Transactions on Energy Conversion*, vol. 28, no. 1, pp. 214–224, 2013, doi: 10.1109/TEC.2012.2228484.

[5] G. Zhang, G. Wang, D. Xu, and N. Zhao, "ADALINE-network-based PLL for position sensorless interior permanent magnet synchronous motor drives," *IEEE Transactions on Power Electronics*, vol. 31, no. 2, pp. 1450–1460, 2016, doi: 10.1109/TPEL.2015.2424256.

[6] A. T. Woldegiorgis, X. Ge, H. Wang, and M. Hassan, "A New Frequency Adaptive Second-Order Disturbance Observer for Sensorless Vector Control of Interior Permanent Magnet Synchronous Motor," *IEEE Transactions on Industrial Electronics*, vol. 0046, no. c, 2020, doi: 10.1109/TIE.2020.3047065.

[7] G. Wang, D. Xiao, N. Zhao, X. Zhang, W. Wang, and D. Xu, "Low-Frequency Pulse Voltage Injection Scheme-Based Sensorless Control of IPMSM Drives for Audible Noise Reduction," *IEEE Transactions on Industrial Electronics*, vol. 64, no. 11, pp. 8415–8426, 2017, doi: 10.1109/TIE.2017.2703875.

[8] H. Li, X. Zhang, C. Xu, and J. Hong, "Sensorless Control of IPMSM Using Moving-Average-Filter Based PLL on HF Pulsating Signal Injection Method," *IEEE Transactions on Energy Conversion*, vol. 35, no. 1, pp. 43–52, 2020, doi: 10.1109/TEC.2019.2946888.

[9] J. M. Liu and Z. Q. Zhu, "Novel Sensorless Control Strategy by Square-Waveform High-Frequency Pulsating Signal Injection Into Stationary Reference Frame," *IEEE Journal of Emerging and Selected Topics in Power Electronics*, vol. 2, no. 2, pp. 171–180, 2014, doi: 10.1109/JESTPE.2013.2295395.

[10] T. Szalai, G. Berger, and J. Petzoldt, "Stabilizing sensorless control down to zero speed by using the high-frequency current amplitude," *IEEE Transactions on Power Electronics*, vol. 29, no. 7, pp. 3646–3656, 2014, doi: 10.1109/TPEL.2013.2279405.

[11] M. Seilmeier, S. Ebersberger, and B. Piepenbreier, "Sensorless Control of PMSM for the Whole Speed Range Using Two-Degree-of-Freedom Current Control and HF Test Current Injection for Low-Speed Range," *IEEE Transactions on Industry Applications*, vol. 51, no. 3, pp. 2268–2278, 2015, doi: 10.1109/TIA.2014.2369828.

[12] Q. Tang, A. Shen, X. Luo, and J. Xu, "IPMSM Sensorless Control by Injecting Bidirectional Rotating HF Carrier Signals," *IEEE Transactions on Power Electronics*, vol. 33, no. 12, pp. 10698–10707, 2018, doi: 10.1109/TPEL.2018.2811126.

[13] Q. Tang, A. Shen, X. Luo, and J. Xu, "PMSM Sensorless Control by Injecting HF Pulsating Carrier Signal into ABC Frame," *IEEE Transactions on Power Electronics*, vol. 32, no. 5, pp. 3767–3776, 2017, doi: 10.1109/TPEL.2016.2583787.

[14] Q. Tang, A. Shen, X. Luo, and J. Xu, "PMSM Sensorless Control by Injecting HF Pulsating Carrier Signal into Estimated Fixed-Frequency Rotating Reference Frame," *IEEE Transactions on Power Electronics*, vol. 32, no. 5, pp. 3767–3776, 2017, doi: 10.1109/TPEL.2016.2583787.

[15] S. Smo and F. Pll, "Position-Estimation Deviation-Suppression Technology of PMSM Combining Phase," vol. 9, no. 1, pp. 335–344, 2021.

[16] G. Wang, H. Zhan, G. Zhang, X. Gui, D. Xu, and S. Member, "Adaptive Compensation Method of Position Estimation Harmonic Error for EMF-Based Observer in Sensorless IPMSM Drives," vol. 29, no. 6, pp. 3055–3064, 2014.

[17] Y. Zhang and J. Liu, "An improved Q-PLL to overcome the speed reversal problems in sensorless PMSM drive," *2016 IEEE 8th International Power Electronics and Motion Control Conference, IPEMC-ECCE Asia 2016*, pp. 1884–1888, 2016, doi: 10.1109/IPEMC.2016.7512582.

[18] Y. Li, H. Lu, W. Qu, S. Sheng, and Z. Wang, "Sensorless Control ofPMSM Based on Low Frequency Voltage Injection at Low Speeds and Standstill," no. 6, pp. 781–787, 2013.

[19] L. Sheng, W. Li, Y. Wang, M. Fan, and X. Yang, "Sensorless Control of a Shearer Short-Range Cutting Interior Permanent Magnet Synchronous Motor Based on a New Sliding Mode Observer," *IEEE Access*, vol. 5, pp. 18439–18450, 2017, doi: 10.1109/ACCESS.2017.2734699.

[20] F. Zhang, S. Dong, J. Wang, Z. He, and Q. Zhang, "A Novel Signal Processing Method of Sliding Mode Observer for Position Sensorless PMSM Drives," in *2019 14th IEEE Conference on Industrial Electronics and Applications (ICIEA)*, Jun. 2019, vol. 11, no. 1, pp. 2479–2484. doi: 10.1109/ICIEA.2019.8834165.